Journal of Materials Chemistry C

ROYAL SOCIETY OF CHEMISTRY

PAPER

View Article Online
View Journal | View Issue

Check for updates

Cite this: *J. Mater. Chem. C*, 2024, **12**, 12847

Hexacoordinate germanate metal–organic frameworks for the detection of Pb^{2+} ions in aqueous solution†

Shouyi Tian, [a] Peter N. Horton,[b] Simon J. Coles, [b] Andrew J. P. White,[a] Paul D. Lickiss [a] and Robert P. Davies *[a]

Received 25th April 2024,
Accepted 12th July 2024

DOI: 10.1039/d4tc01700e

rsc.li/materials-c

Hexacoordinate silicate and germanate linkers supporting high negative charges have been prepared and applied as building blocks for anionic MOF frameworks with lanthanide metal-based nodes. The SiO_6/GeO_6 centred linkers $[Et_3NH]_2[H_3$**L-Si/Ge**$]$ [H_3**L-Si/Ge** = tris(3,4-diolato-benzoic acid) silicate/germanate] were initially prepared and characterised, with the germanate ligand demonstrating excellent water stability. A series of rare earth MOFs (**IMP-33-Sc** and **IMP-34-Ln**, Ln = Y, Gd, Tb, Dy, Ho, Er, Tm, Yb, Lu) were then synthesised under hydrothermal conditions using H_3**L-Ge**. Both **IMP-33-Sc** and **IMP-34-Ln** exhibit (3,6)-connected networks with the same *flu*-3,6-*C*2/*c* topology, however, whereas **IMP-33-Sc** contains trimetallic nodes, **IMP-34-Ln** nodes are bimetallic, thus leading to a higher anionic network charge of 4− in **IMP-34-Ln** (*vs.* 1− in **IMP-33-Sc**). The terbium based MOF **IMP-34-Tb** exhibits characteristic luminescent properties and is shown to be selectively quenched by Pb^{2+} ions in aqueous solutions through a dynamic quenching process. A strong linear relationship between the fluorescence intensity and Pb^{2+} concentration in the range of 0.01–4 mM makes it a promising sensor for aqueous Pb^{2+} ions.

Introduction

Metal–organic frameworks (MOFs) are highly crystalline porous materials with a wide range of potential applications in areas such as gas capture and storage, catalysis, chemical sensing, and water harvesting.[1] The large diversity in these materials is often attributed to the versatility of the organic ligand, which can be designed to impart specific connectivity or functionality. Tetravalent silicon, and to a lesser extent germanium, centred connectors have shown promise in MOF construction as highly branched building blocks,[2–5] and in the case of siloxanes for their high hydrophobicity.[6] Hexavalent silicate and germanate connectors, most notably the hexafluorides SiF_6^{2-} and GeF_6^{2-}, have also been utilized as building blocks for MOF synthesis, in particular in the SIFSIX/GeFSIX series of MOFs.[7–11] These MOFs consist of a 2D-layer comprising di-topic N-based ligands and metal nodes (usually Cu^{2+}, Zn^{2+} or Ni^{2+}), connected to form a 3D network by axial Si/GeF_6^{2-} anions (Fig. 1a).[9] The pore size in these materials can be varied by adopting different length N-donor ligands. Using this approach SIFSIX/GeFSIX MOFs have been successfully optimised for a range of gas storage and separation scenarios.[11–14]

Hexacoordinated Si and Ge connectors based on SiO_6 or GeO_6 octahedra are less well known, with only a handful of examples reported in the MOF and COF literature. The majority of these are based on triscatechol silicate or germanate anions. Martsinko *et al.* have reported two coordination polymers (CPs) with ligands based on GeO_6 octahedra (see Fig. 1b) with Cu^{2+} and Ba^{2+} metal nodes.[15,16] Roeser *et al.* reported two 3D anionic COFs with permanent porosity based on SiO_6 octahedra (Fig. 1c and d).[17,18] An analogous COF with GeO_6 octahedra (Fig. 1d) has also been reported by Wang *et al.*[19]

These connectors are usually highly negatively charged due to the presence of the dianionic hexacoordinate Si or Ge centre. This can bring some unique features to MOF and COF construction including easier access to anionic networks. For example, the presence of alkaline metal counter-cations in the anionic Ge-COFs reported by Wang facilitated fast ion conduction and also increased CO_2 gas selectivity.[19,20] Triscatecholate silicate derivatives have also been used in polymer synthesis and have been studied for absorption of dyes and used as solid electrolytes.[21–23] In this work we focus upon the development of a novel ligand for MOF construction based on SiO_6 or GeO_6 octahedral with tris-connectivity *via* three pendant

[a] *Molecular Sciences Research Hub, Department of Chemistry, Imperial College London, White City, London, W12 0BZ, UK. E-mail: r.davies@imperial.ac.uk*

[b] *EPSRC Crystallographic Service, Department of Chemistry, University of Southampton, Highfield, Southampton, SO17 1BJ, UK*

† Electronic supplementary information (ESI) available. CCDC 2331262 and 2348717–2348719. For ESI and crystallographic data in CIF or other electronic format see DOI: https://doi.org/10.1039/d4tc01700e

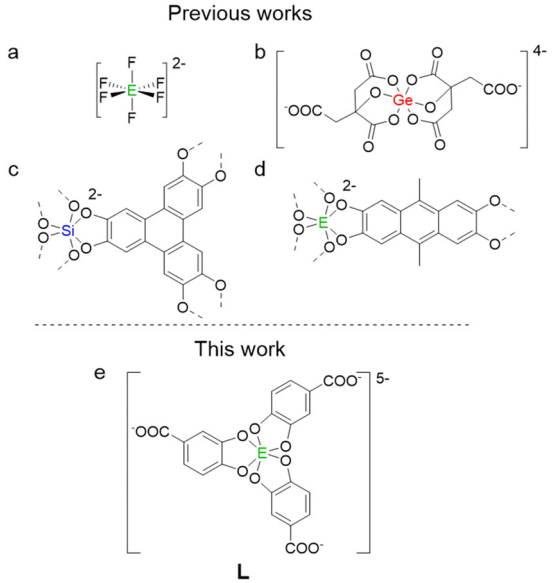

Fig. 1 (a)–(e) Hexavalent Si/Ge connectors used in MOF and COF construction (E = Si/Ge).

carboxylate groups and an overall 5− negative charge (Fig. 1e). It was anticipated that these building blocks could facilitate the formation of MOF networks with more highly charged metal centres (such as rare earth cations) and also aid in the formation of novel anionic frameworks with potential use in the detection or absorption of cationic species such as Pb^{2+}.[24]

Lead is a commonly encountered toxic element because it will accumulate in the human body and cause permanent damage to the nervous system even at low concentrations.[25] Exposure to lead has also been linked to various diseases such as cancer, and anaemia.[26] As such, there is high interest in the development of sensitive sensors for detecting lead in aqueous solutions. Lanthanide elements are well known for optical sensing with characteristic luminescent emission.[27,28]

In the present work, the triethylammonium salts of novel tris-catechol silicate/germanate type ligands, namely $[Et_3NH]_2[H_3$**L-Si/Ge**$]$, have been synthesised. These contain three pendant carboxylic acid groups which can provide coordination sites for metal cations in MOF construction (Fig. 1e). Unlike the silicon-based connector, the germanium-based linker was shown to have excellent water stability and was used to prepare a series of GeO_6-based MOFs with rare earth (RE) metals which exhibited novel 3D structures and good water stability. Among these MOFs, **IMP-34-Tb** emitted bright green light under UV excitation and showed promise in Pb^{2+} sensing.

Experimental section

Materials and general methods are specified in the ESI.†

Linker synthesis

Bis(triethylammonium) tris(3,4-diolato-benzoic acid) silicate $[Et_3NH]_2[H_3$**L-Si**$]$: 3,4-dihydroxybenzoic acid (2.312 g, 15 mmol) was first dissolved in acetonitrile (20 mL). Et_3N (1.39 mL, 10 mmol) was added to the stirred solution, resulting in the formation of a white precipitate. $Si(OMe)_4$ (0.74 mL, 5 mmol) was then added, and the mixture was stirred at room temperature for 48 h. The white precipitate formed was isolated by suction filtration, then washed with acetonitrile and diethyl ether before drying under vacuum at 50 °C for 3 h to give a white powder. Yield: 2.92 g, 85%. ^{1}H NMR (400 MHz, D_6-DMSO): δ (ppm) = 10.51 (br, 1H, COO**H**), 7.10 (dd, 1H, J = 8, 2 Hz, C6-**H**), 6.79 (t, 1H, J = 2 Hz, C2-**H**), 6.26 (d, 1H, J = 8 Hz, C5-**H**), 3.10 (q, 4H, J = 8 Hz, C$\mathbf{H}_2$CH$_3$), 1.16 (t, 6H, J = 8 Hz, CH$_2$C$\mathbf{H}_3$); ^{13}C NMR (101 MHz, D_6-DMSO): δ (ppm) = 168.99 (**C**OOH), 157.91, 151.83, 120.43, 117.74, 109.59, 108.69, 46.30 (**C**H$_2$CH$_3$), 9.12 (CH$_2$**C**H$_3$); ^{29}Si NMR (80 MHz, D_6-DMSO): δ (ppm) = −138.17; MS (ESI†): calcd (monoisotopic) for $[C_{21}H_{12}O_{12}Si + H]^-$ m/z = 485.0182, found m/z = 485.0198; IR (ATR): ν (cm^{-1}) = 2980 (br), 1656, 1498, 1444, 1269, 1118, 829, 774, 691, 663, 543.

Bis(triethylammonium) tris(3,4-diolato-benzoic acid) germanate $[Et_3NH]_2[H_3$**L-Ge**$]$: 3,4-dihydroxybenzoic acid (1.849 g, 12 mmol) was dissolved in acetonitrile (dry solvent, 20 mL). Et_3N (1.12 mL, 8 mmol) was added to the stirred solution, resulting in the formation of a white precipitate. $Ge(OMe)_4$ (0.59 mL, 4 mmol) was then added, and the mixture was stirred at room temperature for 48 h. The resulting white precipitate was isolated by suction filtration, then washed with acetonitrile and diethyl ether before drying under vacuum at 50 °C for 3 h to give a white powder. Yield: 2.73 g, 93%. ^{1}H NMR (400 MHz, D_2O): δ (ppm) = 7.31 (dd, 1H, J = 8 Hz, C6-**H**), 7.18 (d, 1H, J = 2 Hz, C2-**H**), 6.64 (d, 1H, J = 8 Hz, C5-**H**), 2.99 (q, 4H, J = 8 Hz, C$\mathbf{H}_2$CH$_3$), 1.10 (t, 6H, J = 8 Hz, CH$_2$C$\mathbf{H}_3$); ^{13}C NMR (101 MHz, D_2O): δ (ppm) = 171.38 (**C**OOH), 154.74, 148.36, 122.23, 118.48, 112.34, 111.66, 46.59 (**C**H$_2$CH$_3$), 8.15 (CH$_2$**C**H$_3$); MS (ESI†): calcd for $[C_{21}H_{12}O_{12}Ge + H]^-$ m/z = 530.9624, found m/z = 530.9626; IR (ATR): ν (cm^{-1}) = 3010 (br), 1657, 1494, 1439, 1264, 1118, 942, 813, 773, 648, 408.

Synthesis of MOFs

A mixture of metal nitrate (Sc, Y, Gd, Tb, Dy, Ho, Er, Tm, Yb or Lu, all trivalent, 0.1 mmol) and $[Et_3NH]_2[H_3$**L-Ge**$]$ (0.05 mmol) were placed in a 7 mL screw cap glass vial, followed by addition of water (3 mL) and MeCN (1 mL). The mixture was sealed and sonicated for 5 min to ensure the reagents completely dissolved, before heating at 80 °C for 24 h to afford blade-shaped crystals (except for **IMP-33-Sc** which gave prism-shaped crystals). **IMP-34-Ho** and **IMP-34-Er** gave pale orange and pink crystals respectively, whilst all other crystals were colourless. Crystals were isolated from the hot solution directly through filtration, and the bulk phase purity of the crystals was confirmed through PXRD measurements (Fig. 5 and Fig. S3, ESI†).

Results and discussion

Synthesis and general characterization

The $[H_3$**L-Si/Ge**$]^{2-}$ linkers were synthesized as triethyl-ammonium salts from the reaction of 3,4-dihydroxybenzoic with Et_3N and

either $Si(OMe)_4$ or $Ge(OMe)_4$, using a similar procedure to that previously employed for tris(catecholate) silicate/germanate synthesis (Scheme 1).[29] The successful preparation of the desired hexacoordinate SiO_6/GeO_6 based linkers was confirmed using multinuclear NMR and IR spectroscopy and mass spectrometry. ^{1}H NMR studies on both Si and Ge linkers were consistent with the formation of the products with a 1 : 2 ratio of silicate/germanate anion to ammonium cation. ^{29}Si NMR studies on $[H_3$**L-Si**$]^{2-}$ gave a single peak at −138.2 ppm which is close to that previously reported for tris(catecholate) silicate (−141.2 ppm).[29]

The silicon-based H_3**L**-Si dianion showed poor water stability: dissolution in water was followed by precipitation of a white powder (presumably silicon dioxide[30]) and ^{29}Si NMR spectra revealed no silicon-containing species remained in the solution. Additionally, ^{1}H NMR (in D_2O) showed regeneration of the 3,4-dihydroxybenzoic acid starting material indicating full hydrolysis of $[H_3$**L**-Si$]^{2-}$ had occurred.[29] In contrast H_3**L**-Ge showed no evidence of decomposition in the presence of water even when heated in D_2O at 80 °C for 72 hours (see ESI†).

Solid-state structure of $[Et_3NH]_2[H_3$**L-Si**$]$

Slow diffusion of diethyl ether into a dry DMF solution of $[Et_3NH]_2[H_3$**L-Si**$]$ afforded colourless tablet crystals which were analysed using single-crystal X-ray diffraction. In addition to the ligand structure, we were interested to see whether this silicate could form a hydrogen bonding network (HOF).[31]

$[Et_3NH]_2[H_3$**L-Si**$]$ crystallised in the triclinic $P\bar{1}$ space group, with the silicon atom coordinated by three deprotonated catecholate groups as expected to give a slightly distorted octahedral geometry at Si, as shown in Fig. 2a. The Si–O bond lengths are in the range 1.767(3) to 1.798(3) Å, with adjacent and opposite O–Si–O bond angles in the ranges 87.10(14) to 94.67(14)° and 174.50(16) to 177.24(16)° respectively. These values are consistent with those reported for other tris-catechol silicate species.[29,32] In addition, the dianion is chiral at the Si centre, with a racemic mix of D- and L-isomers observed in the solid-state structure.

Intermolecular H-bonds are observed between the N–H group on the ammonium cation and three facially positioned oxygen atoms in the SiO_6 group. The N(H)···O–Si distances are in the range 2.867 and 3.355 Å (mean 3.146 Å). Two of the carboxylic acid groups in the H_3**L-Si** dianion form hydrogen bonding dimers with adjacent COOH groups, resulting in the formation of a zigzag H-bonded chain (Fig. 2b). The O(H)···O

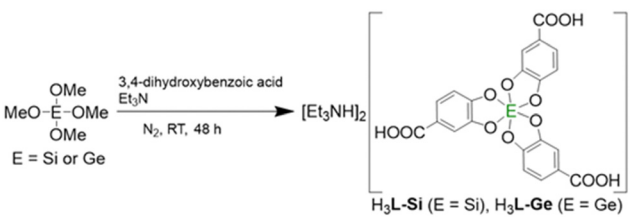

Scheme 1 Linker synthesis.

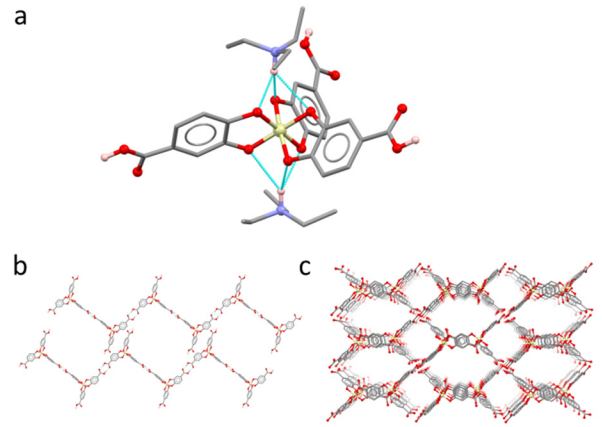

Fig. 2 (a) Crystal structure of $[Et_3NH]_2[H_3$**L-Si**$]$; (b) zigzag H-bonding chain structure; (c) packing diagram viewed along (0 1 0); C: grey, H: pink, O: red, N: light blue, Si: pale yellow; H bonds are shown as light blue lines; alkyl/aryl H atoms and ammonium cations in (b) and (c) are omitted for clarity.

distances range between 2.573 and 2.605 Å, which are consistent with similar structures in HOFs built from poly-carboxylic acids.[4] The third carboxylic acid group does not participate in hydrogen bonding with other silicate or ammonium ions.

The 1D hydrogen-bonded chains pack in an antiparallel fashion in the crystal lattice to give a structure with channels of diameter 3.4 Å along the (0 1 0) direction[33] (Fig. 2c). However, these potential void areas are filled with ammonium cations and disordered solvent molecules (calculated three DMF per formula unit). The absence of a robust 3D H-bonding network meant it was not possible to remove the solvent molecules and realize any permanent porosity for this material.

Although it was not possible to obtain crystals of $[Et_3NH]_2$ $[H_3$**L-Ge**$]$ suitable for SCXRD characterisation, the PXRD pattern for this compound matches closely with the PXRD pattern obtained for $[Et_3NH]_2[H_3$**L-Si**$]$ (Fig. S1, ESI†), indicative of their isostructural nature.

IMP-33-Sc

Attempts to prepare novel MOFs with the $[H_3$**L-Si**$]^{2-}$ silicate linker was unsuccessful due to the poor water stability of this molecule (*vide supra*). However, the good water stability of the germanate linker allowed a series of MOFs to be prepared using $[Et_3NH]_2[H_3$**L-Ge**$]$. Thus, the reaction of $[Et_3NH]_2[H_3$**L-Ge**$]$ with $Sc(NO_3)_3$ in a mixture of water and MeCN at 80 °C for 24 h afforded colourless prism-shaped crystals. Single crystal X-ray diffraction revealed a 3D MOF network of structure $[Sc_3$(**L-Ge**$)_2(H_2O)_6]\cdot[Et_3NH]\cdot(MeCN)_6(H_2O)_9$ (**IMP-33-Sc**), and the purity of the bulk sample was confirmed by PXRD measurements (Fig. S2, ESI†). **IMP-33-Sc** crystallised in the monoclinic space group $P2_1$ as an anionic framework, with triethylammonium cations and disordered solvent molecules (MeCN and H_2O) sited within the pores. The triethylammonium cations were located in the crystal structure and form H-bonding interactions between the ammonium N–H and two O different atoms from the GeO_6 centre, with the distances

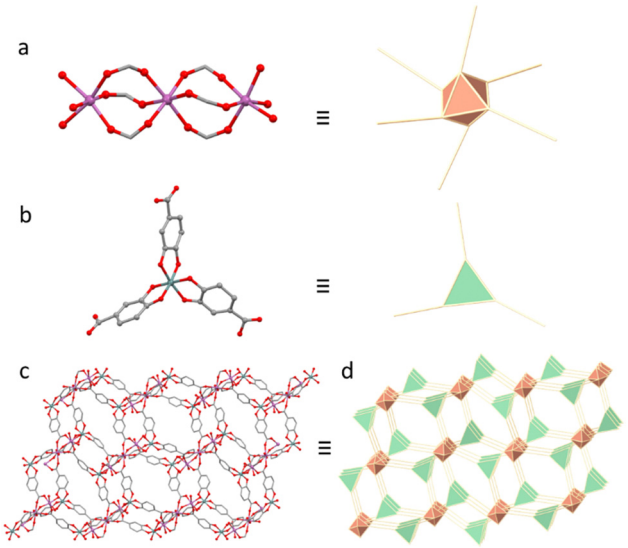

Fig. 3 (a) Coordination environment of the SBU; (b) tridentate Ge ligand; (c) packing diagram of the **IMP-33-Sc** (0 1 0); (d) topology view of the network. C: grey, O: red, Ge: grey blue, Sc: pink, H atoms are omitted for clarity.

ranging from 2.988 to 3.264 Å. H-Bonding interactions are also observed to the GeO_6 unit from the metal coordinating water molecules in the SBU (Fig. S16, ESI†). Furthermore, ^{1}H NMR spectra of the digested MOF in aqueous NaOD confirms the triethylammonium to **L-Ge** ratio of 1 : 2 (Fig. S13, ESI†).

To visualise the topology of the framework better, the metal clusters and ligands can be reduced to simple nodes (Fig. 3). There are two types of crystallographically independent metal-containing nodes or SBUs which both exhibit the same connectivity being based on three linearly arranged Sc^{3+} cations with octahedral geometries (Fig. S17, ESI†). The central Sc^{3+} cations coordinate with six bridging di-monodentate carboxylate groups (each from a different ligand), while the terminal Sc^{3+} cations coordinate with three bridging di-monodentate carboxylate groups and three water molecules (Fig. 3a). Similar motifs are well known in transition metal-based MOFs and have been previously reported for Sc with different terminal coordinated molecules.[34] There are four types of crystallographic distinct germanate molecules, each of which bridges three metal SBUs in a $(\kappa^1\text{-}\kappa^1\text{-}\mu_2)^3\text{-}\mu_6$ coordination mode. The combination of 6-connected metal nodes and 3-connected ligands yields a *flu*-3,6-*C*2/*c* topology, which is somewhat rare in the literature but has been previously reported in a series of MOFs using tridentate carboxylate linkers and lanthanide metal clusters.[35–38]

Theoretical removal of disordered non-coordinated solvent molecules, coordinated water molecules and ammonium cations from the pores of **IMP-33-Sc** gave a PLATON[39] predicted solvent-accessible void volume of 57% of the unit cell. However, **IMP-33-Sc** became amorphous after activation under vacuum at 60 °C for 12 h, as indicated by PXRD (Fig. S2, ESI†). This was attributed to the partial collapse of the framework, and thus the material did not exhibit any permanent microporosity. However, soaking the 'activated' MOF in water led to the regeneration of **IMP-33-Sc** as shown using PXRD (Fig. S2, ESI†).

IMP-34-Y and IMP-34-Ln

A series of lanthanide metal nitrates (Y, Gd, Tb, Dy, Ho, Er, Tm, Yb or Lu, all trivalent) were treated with $[Et_3NH]_2[H_3$**L-Ge**$]$ in a mixture of water and MeCN in a sealed glass vial at 80 °C for 24 h to afford blade-shape crystals in each case. The yttrium containing crystals were analysed by SCXRD and found to be $[Y_2(\textbf{L-Ge})_2(H_2O)_4][Y(H_2O)_8][Et_3NH]\cdot 3H_2O$. **IMP-34-Y** crystallised in the monoclinic space group *C*2/*c* and comprises an anionic $[Y_2(\textbf{L-Ge})_2(H_2O)_4]^{4-}$ network counterbalanced by $[Y(H_2O)_8]^{3+}$ and $[Et_3NH]^+$ cations within its pores. The oxygen atoms in the GeO_6 centre form hydrogen bonds to coordinated water molecules of the $[Y(H_2O)_8]^{3+}$ counter-cation as well as to solvent water molecules (Fig. S18, ESI†). H-Bond interactions were also observed between the oxygen atoms on the ligand carboxylate groups and water molecules from solvent and SBU. The solvated Y^{3+} counter cation was located in the solid-state structure, however the ammonium cations were not observed due to disorder although their presence was confirmed using ^{1}H NMR spectroscopy of the digested MOF in aqueous NaOD which showed a germanate ligand to ammonium cation ratio of 2 : 1 (Fig. S14, ESI†).

The metal nodes (SBUs) in **IMP-34-Y** comprise two yttrium cations, each of which is coordinated by two bidentate chelating carboxylate groups, two di-monodentate bridging carboxylate groups and two water molecules (Fig. 4a). This therefore gives a six-connected vertex. The three deprotonated carboxylate groups in each ligand molecule bind to a different SBU to give an overall $(\kappa^1\text{-}\kappa^1\text{-}\mu_1)^2\text{-}(\kappa^1\text{-}\kappa^1\text{-}\mu_2)\text{-}\mu_4$ coordination mode. To visualise the topology of the framework better, the metal clusters and ligands can be reduced to simple 6- and 3-connected nodes respectively (Fig. 4) to give a *flu*-3,6-*C*2/*c*

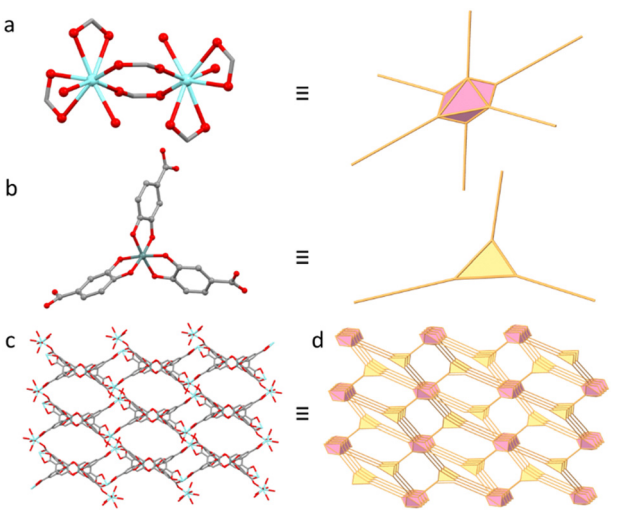

Fig. 4 (a) Coordination environment of the SBU; (b) tridentate Ge ligand; (c) packing diagram of the **IMP-34-Y** (0 1 0); (d) topology view of the network (0 1 0). C: grey, O: red, Ge: grey blue, Y: pale blue. H atoms are omitted for clarity.

network. Interestingly, this is the same topology as observed in **IMP-33-Sc**, however the bimetallic metal node in **IMP-34-Y** has a lower charge than the trianionic metal node in **IMP-33-Sc** resulting in a higher negative charge on the network: $[Y_2(\textbf{L-Ge})_2]^{4-}$ *vs.* $[Sc_3(\textbf{L-Ge})_2]^{-}$.

Powder X-ray diffraction measurements on freshly prepared **IMP-34-Y** show the bulk product to be consistent with the calculated pattern from the single crystal X-ray data (Fig. S3, ESI†). Theoretical removal of highly disordered non-coordinated solvent molecules and cations from the pores of **IMP-34-Y** gave an estimated solvent-accessible void volume of 59% using PLATON.[39] However, N_2 sorption studies on the activated material (heated under vacuum at 60 °C for 12 h) revealed that the framework is essentially non-porous, presumably due to the presence of metal and ammonium cations in the pore space which could not be removed under vacuum (Fig. S19, ESI†). Activation of **IMP-34-Y** resulted in some minor peak shifts, however soaking the activated MOF in water led to the regeneration of the original MOF material as shown using PXRD studies (Fig. S3, ESI†) and demonstrated the stability of the MOF under aqueous conditions.

Single crystal analysis of **IMP-34-Dy** reveals that this MOF has an identical framework structure and topology to **IMP-34-Y**, with minor differences in unit cell parameters (Fig. S20, S21 and Table S2, ESI†). All the other lanthanide MOFs studied were shown to have matching PXRD patterns to **IMP-34-Y** and **IMP-34-Dy** (Fig. 5) and hence are predicted to be isostructural.[40] Thermogravimetric analysis of all **IMP-34-Ln** MOFs exhibited similar weight loss curves (Fig. S4, ESI†), with thermal stability up to 300 °C.

Photoluminescence properties of IMP-34-Tb

Tb-based MOFs have been reported to exhibit outstanding luminescent properties with a visible region light emission, and have been used in a variety of sensing applications.[41–44] **IMP-34-Tb** displays a bright green luminescence in the solid state under UV excitation (366 nm). The luminescence property was studied in aqueous suspension by adding 3 mg **IMP-34-Tb** to 3 mL DI water, followed by treatment in an ultrasound bath for 20 min. **IMP-34-Tb** exhibits characteristic luminescence emission peaks at 488 nm, 545 nm, 585 nm and 621 nm (λ_{ex} = 330 nm, Fig. 6) corresponding to the typical f–f transitions of Tb^{3+} ions ($^5D_4 \rightarrow {}^7F_6$, $^5D_4 \rightarrow {}^7F_5$, $^5D_4 \rightarrow {}^7F_4$ and $^5D_4 \rightarrow {}^7F_3$ respectively). The absolute quantum yield of the **IMP-34-Tb** is found to be 24.45%, and the average fluorescence lifetime is 0.65 ms (Fig. S5, ESI†).

Sensing of Pb^{2+} ions

We then proceeded to study the sensing ability of the **IMP-34-Tb** towards metal ions, with a view to its application as a sensor for aqueous Pb^{2+}. A series of aqueous solutions (metal nitrate) containing either Na^+, Mg^{2+}, K^+, Ca^{2+}, Mn^{2+}, Co^{2+}, Ni^{2+}, Zn^{2+}, Sr^{2+}, Cd^{2+}, Cs^+ or Pb^{2+} ions were prepared with a concentration of 10 mM. When the **IMP-34-Tb** MOF was added to the Pb^{2+} solution there was a significant fluorescence quench (90%), while other metal ions did not markedly affect the intensity (Fig. 7, quench percentage = $[(I_0 - I)/I_0] \times 100\%$, I_0 and I are the luminescence intensity of the $^5D_4 \rightarrow {}^7F_5$ transitions (545 nm) of **IMP-34-Tb** before and after treatment with metal cations respectively). This phenomenon suggests that the **IMP-34-Tb** can be used to selectively detect Pb^{2+} ions in aqueous solutions.

The sensing sensitivity of **IMP-34-Tb** towards Pb^{2+} ions was then studied using various concentrations of Pb^{2+} solutions. The fluorescence emission intensity decreased with the increasing Pb^{2+} concentration (Fig. 7b). The quench efficiency was calculated with the Stern–Volmer equation, $I_0/I = 1 + K_{SV}[Q]$, where K_{SV} is the quenching constant, and [Q] is the concentration of the Pb^{2+} ion.[44] The plot shown in Fig. 7b reveals a linear relationship (R^2 = 0.994) between relative intensity and Pb^{2+} concentration in the range of 10^{-2} mM to 4 mM. The calculated K_{SV} value is 1.80×10^3 M^{-1}, which is comparable to other MOFs which have been reported for Pb^{2+} ion sensing (Table 1). The calculated limit of detection (LOD = $3\sigma/K_{SV}$, where σ is the standard error) is 2.29×10^{-4} M.

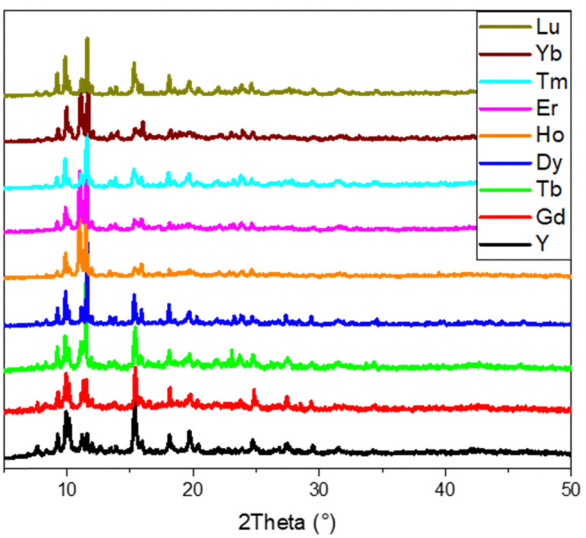

Fig. 5 PXRD results of **IMP-34-Y** and **IMP-34-Ln**.

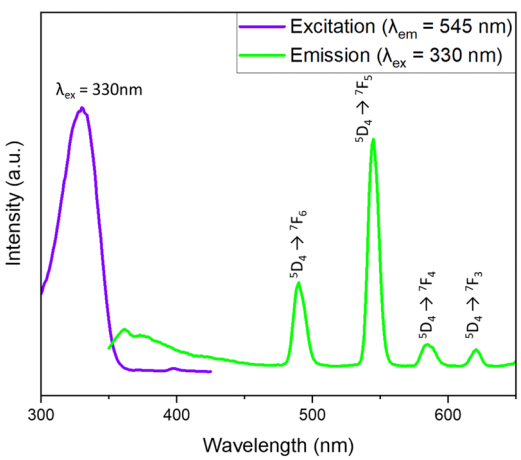

Fig. 6 Excitation and emission spectra of **IMP-34-Tb**.

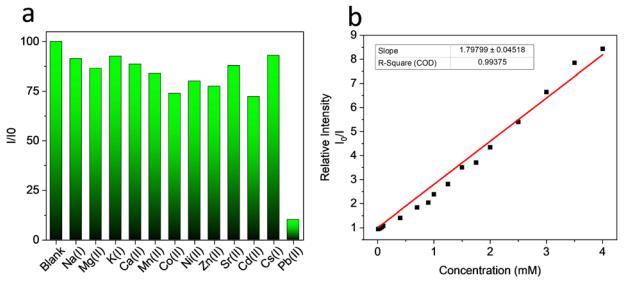

Fig. 7 (a) Relative luminescence intensity of **IMP-34-Tb** at 545 nm with different metal cations; (b) linear relationship between the relative luminescence intensity and Pb^{2+} concentration at 545 nm.

The efficacy of **IMP-34-Tb** for Pb^{2+} sensing in the presence of multiple metal ions was also evaluated by using a solution containing a cocktail of metal ions (10 mM: Na^+, Mg^{2+}, K^+, Ca^{2+}, Mn^{2+}, Co^{2+}, Ni^{2+}, Zn^{2+}, Cd^{2+}, Sr^{2+} and Cs^+). The luminescence intensity of **IMP-34-Tb** was higher than 90% in the mixed ion solution in the absence of Pb^{2+} ions, however on addition of Pb^{2+} the luminescent intensity fell to below 10% (Fig. S7, ESI†). These results are promising, showing good performance under conditions commonly encountered in environmental and biological systems.

Quench mechanism

In order to investigate the quench mechanism in the low concentration regime, the luminescent lifetime of **IMP-34-Tb** before and after treatment with Pb^{2+} (0.1 mM) was measured. The result shows that on treatment with the Pb^{2+} solution, there was a noticeable decrease in the phosphorescence lifetime from 0.65 to 0.55 ms (545 nm). Meanwhile, UV-vis absorption results (Fig. S6, ESI†) show that there is no overlap between the absorption band of the Pb^{2+} solution and the excitation/emission bands for **IMP-34-Tb**. These results therefore exclude the possibility of a competitive absorption mechanism. MOF decomposition or the formation of new non-fluorescent complexes during the quench process was ruled out using PXRD results (Fig. S8, ESI†). Hence it can be concluded that a dynamic quench mechanism is occurring. The quench behaviour likely originates from the coordination of the Pb^{2+} ions to the phenolic oxygens in **IMP-34-Tb**, facilitated by the highly negative charge of the framework.[41] Such interactions will affect the energy transfer process between the Tb^{3+} ion and the framework, where the latter acts as the "antenna". Furthermore, after washing the Pb-treated **IMP-34-Tb** with water 3 times, the luminescence intensity of the MOF sample returns to approx. 100% compared to the untreated MOF sample (Fig. S9, ESI†). This phenomenon further verifies the presence of a dynamic quench mechanism at lower concentration regions, as the MOF retains its structure in the quench process.

Table 1 Selection of MOFs reported for Pb^{2+} sensing

MOF	K_{SV}/M^{-1}	Ref.
$[Tb(5\text{-}HiBDC)(H_2O)_5]_n$[a]	1.75×10^4	41
$Cu_2(BDC)_2(bpy)$[b]	3.91×10^3	45
$[Eu_2(FDC)_3DMA(H_2O)_3]\cdot DMA\cdot 4.5H_2O$[c]	2.97×10^3	46
$[[Tb(dppa)(H_2O)_2]\cdot dima\cdot H_2O\cdot 0.5O]_n$[d]	8.69×10^3	42
IMP-34-Tb	1.80×10^3	This work

[a] 5-HiH_2BDC = 5-hydroxy-iso-benzenedicarboxylic acid. [b] H_2bdc = benzene-1,4-dicarboxylic acid, bpy = 4,4′-bipyridine. [c] H_2FDC = 9,9-dimethyl-2,7-fluorenedicarboxylic acid. [d] H_4dppa = 5-(3′4′-dicarboxylphenoxy) isophthalic acid, dima = dimethyl-amine.

Conclusions

In summary, novel silicate and germanate linkers have been prepared based on SiO_6 or GeO_6 octahedra with three pendant carboxylic acid groups and high negative charges of 5− in their deprotonated forms. The Si linker salt $[Et_3NH]_2[H_3$**L-Si**$]$ self-assembles into zigzag chains in the solid state by way of intermolecular H-bonding interactions between neighbouring carboxylic acid functionalities. However, the poor water stability of $[H_3$**L-Si**$]^{2-}$ made it unsuitable for applications in solvothermal MOF synthesis protocols and hence the isostructural but water-stable $[H_3$**L-Ge**$]^{2-}$ was employed instead. Thus, reaction of RE metal nitrates with $[H_3$**L-Ge**$]^{2-}$ gave a series of novel anionic RE-MOFs. Both **IMP-33-Sc** and **IMP-34-Ln** exhibit (3,6)-connected networks with the same *flu*-3,6-*C*2/*c* topology, however whereas **IMP-33-Sc** contains trimetallic nodes, **IMP-34-Ln** nodes are bimetallic, thus leading to a higher anionic network charge of 4− in **IMP-34-Ln** (*vs.* 1− in **IMP-33-Sc**). These materials represent the first examples of MOFs built from tridentate GeO_6 based linkers. Additionally, **IMP-34-Tb** exhibits characteristic luminescence properties and is shown to have good selectivity towards Pb^{2+} ions with potential applications in the quantitative detection of these heavy metal ions in aqueous solutions.

Data availability

The data supporting this article have been included as part of the ESI.† Crystallographic data for compounds $[Et_3NH]_2[H_3$**L-Si**$]$, **IMP-33-Sc**, **IMP-34-Y** and **IMP-34-Dy** have been deposited at Cambridge Crystallographic data centre (CCDC) under 2331262, 2348717, 2348718, and 2348719 respectively and can be obtained *via* https://www.ccdc.cam.ac.uk/structures. Additional information on the data refinements are included in the ESI.†

Conflicts of interest

There are no conflicts to declare.

Acknowledgements

We thank Mr Jiewen Wei for the measurement of quantum yield.

Notes and references

1 M. Ding, R. W. Flaig, H. L. Jiang and O. M. Yaghi, *Chem. Soc. Rev.*, 2019, **48**, 2783–2828.

2 L. C. Delmas, P. N. Horton, A. J. P. White, S. J. Coles, P. D. Lickiss and R. P. Davies, *Chem. Commun.*, 2017, **53**, 12524–12527.
3 L. C. Delmas, A. J. P. White, D. Pugh, P. N. Horton, S. J. Coles, P. D. Lickiss and R. P. Davies, *CrystEngComm*, 2018, **20**, 4541–4545.
4 D. Pugh, E. Ashworth, K. Robertson, L. C. Delmas, A. J. P. White, P. N. Horton, G. J. Tizzard, S. J. Coles, P. D. Lickiss and R. P. Davies, *Cryst. Growth Des.*, 2018, **19**, 487–497.
5 L. C. Delmas, P. N. Horton, A. J. P. White, S. J. Coles, P. D. Lickiss and R. P. Davies, *Polyhedron*, 2019, **157**, 25–32.
6 L. C. Delmas, A. J. P. White, D. Pugh, A. Evans, M. A. Isbell, J. Y. Y. Heng, P. D. Lickiss and R. P. Davies, *Chem. Commun.*, 2020, **56**, 7905–7908.
7 O. Alduhaish, R.-B. Lin, H. Wang, B. Li, H. D. Arman, T.-L. Hu and B. Chen, *Cryst. Growth Des.*, 2018, **18**, 4522–4527.
8 B. Li, X. Cui, D. O'Nolan, H. M. Wen, M. Jiang, R. Krishna, H. Wu, R. B. Lin, Y. S. Chen, D. Yuan, H. Xing, W. Zhou, Q. Ren, G. Qian, M. J. Zaworotko and B. Chen, *Adv. Mater.*, 2017, **29**, 1704210.
9 P. Nugent, Y. Belmabkhout, S. D. Burd, A. J. Cairns, R. Luebke, K. Forrest, T. Pham, S. Ma, B. Space, L. Wojtas, M. Eddaoudi and M. J. Zaworotko, *Nature*, 2013, **495**, 80–84.
10 Z. Zhang, X. Cui, L. Yang, J. Cui, Z. Bao, Q. Yang and H. Xing, *Ind. Eng. Chem. Res.*, 2018, **57**, 7266–7274.
11 T. Ke, Q. Wang, X. Zhu, J. Hu, Z. Bao, Z. Zhang, Q. Ren and Q. Yang, *Chem. Eng. J.*, 2023, **472**, 144852.
12 H. Li, L. Li, R. B. Lin, G. Ramirez, W. Zhou, R. Krishna, Z. Zhang, S. Xiang and B. Chen, *ACS Sustainable Chem. Eng.*, 2019, **7**, 4897–4902.
13 H.-M. Wen, C. Liao, L. Li, A. Alsalme, Z. Alothman, R. Krishna, H. Wu, W. Zhou, J. Hu and B. Chen, *J. Mater. Chem. A*, 2019, **7**, 3128–3134.
14 Y. Jiang, Y. Hu, B. Luan, L. Wang, R. Krishna, H. Ni, X. Hu and Y. Zhang, *Nat. Commun.*, 2023, **14**, 401.
15 A. G. Pesaroglo, E. E. Martsinko, L. K. Minacheva, I. I. Seifullina and V. S. Sergienko, *Russ. J. Inorg. Chem.*, 2010, **55**, 1366–1372.
16 I. I. Seifullina, E. E. Martsinko, E. A. Chebanenko, V. V. D'yakonenko, S. V. Shishkina and O. V. Pirozhok, *J. Struct. Chem.*, 2018, **59**, 154–159.
17 J. Roeser, D. Prill, M. J. Bojdys, P. Fayon, A. Trewin, A. N. Fitch, M. U. Schmidt and A. Thomas, *Nat. Chem.*, 2017, **9**, 977–982.
18 O. Yahiaoui, A. N. Fitch, F. Hoffmann, M. Fröba, A. Thomas and J. Roeser, *J. Am. Chem. Soc.*, 2018, **140**, 5330–5333.
19 S. Ashraf, Y. Zuo, S. Li, C. Liu, H. Wang, X. Feng, P. Li and B. Wang, *Chem. – Eur. J.*, 2019, **25**, 13479–13483.
20 S. Ashraf, C. Liu, S. Li, I. U. Haq, M. Mehmood, P. Li and B. Wang, *ACS Appl. Mater. Interfaces*, 2020, **12**, 40372–40380.
21 G. Xiong, B.-B. Wang, L.-X. You, B.-Y. Ren, Y.-K. He, F. Ding, I. Dragutan, V. Dragutan and Y.-G. Sun, *J. Mater. Chem. A*, 2019, **7**, 393–404.
22 H. Luo, G. S. H. Poon Ho, C. Li, J. Huang, Z.-L. Xu and Y. Kim, *Ind. Eng. Chem. Res.*, 2023, **62**, 15790–15797.
23 C. Li, D. D. Wang, G. S. H. Poon Ho, Z. Zhang, J. Huang, K. T. Bang, C. Y. Lau, S. Y. Leu, Y. Wang and Y. Kim, *J. Am. Chem. Soc.*, 2023, **145**, 24603–24614.
24 T. Sun, R. Fan, R. Xiao, T. Xing, M. Qin, Y. Liu, S. Hao, W. Chen and Y. Yang, *J. Mater. Chem. A*, 2020, **8**, 5587–5594.
25 F. Wang, F. Zhang, Z. Zhao, Z. Sun, Y. Pu, Y. Wang and X. Wang, *Dalton Trans.*, 2021, **50**, 12197–12207.
26 H. Zhu, J. Yuan, X. Tan, W. Zhang, M. Fang and X. Wang, *Environ. Sci.: Nano*, 2019, **6**, 261–272.
27 S. N. Zhao, G. Wang, D. Poelman and P. Van Der Voort, *Materials*, 2018, **11**, 572.
28 Y. Cui, B. Chen and G. Qian, *Coord. Chem. Rev.*, 2014, **273–274**, 76–86.
29 R. Tacke, A. Stewart, J. Becht, C. Burschka and I. Richter, *Can. J. Chem.*, 2000, **78**, 1380–1387.
30 J. V. Kingston and J. G. Verkade, *Inorg. Chem. Commun.*, 2005, **8**, 643–646.
31 B. Wang, R. B. Lin, Z. Zhang, S. Xiang and B. Chen, *J. Am. Chem. Soc.*, 2020, **142**, 14399–14416.
32 P. Bindu, B. Varghese and M. N. S. Rao, *Phosphorus, Sulfur Silicon Relat. Elem.*, 2003, **178**, 2373–2386.
33 Calculated based on VdW radii using Cavities routine of CrystalMaker®: a crystal and molecular structures program for Mac and Windows, CrystalMaker Software Ltd, Oxford, England, **https://www.crystalmaker.com**.
34 H.-J. Lv, S.-C. Fan, Y.-C. Jiang, S.-N. Li and Q.-G. Zhai, *Inorg. Chem. Front.*, 2023, **10**, 3015–3024.
35 J. Xu, L. Sun, H. Xing, Z. Liang, J. Yu and R. Xu, *Inorg. Chem. Commun.*, 2011, **14**, 978–981.
36 S. Su, S. Wang, X. Song, S. Song, C. Qin, M. Zhu, Z. Hao, S. Zhao and H. Zhang, *Dalton Trans.*, 2012, **41**, 4772–4779.
37 C. Zhang, Y. Yan, Q. Pan, L. Sun, H. He, Y. Liu, Z. Liang and J. Li, *Dalton Trans.*, 2015, **44**, 13340–13346.
38 D. Wang, L. Sun, C. Hao, Y. Yan and Z. Liang, *RSC Adv.*, 2016, **6**, 57828–57834.
39 A. L. Spek, *J. Appl. Crystallogr.*, 2003, **36**, 7–13.
40 Á. Monge, F. Gándara, E. Gutiérrez-Puebla and N. Snejko, *CrystEngComm*, 2011, **13**, 5031–5044.
41 G. Ji, J. Liu, X. Gao, W. Sun, J. Wang, S. Zhao and Z. Liu, *J. Mater. Chem. A*, 2017, **5**, 10200–10205.
42 X.-L. Chen, L. Shang, L. Liu, H. Yang, H.-L. Cui and J.-J. Wang, *Dyes Pigm.*, 2021, **196**, 109809.
43 X. Y. Zhao, H. Yang, W. Y. Zhao, J. Wang and Q. S. Yang, *Dalton Trans.*, 2021, **50**, 1300–1306.
44 X. Lu, Y. Tang, G. Yang and Y.-Y. Wang, *J. Mater. Chem. C*, 2023, **11**, 2328–2335.
45 E. Moradi, R. Rahimi and V. Safarifard, *J. Solid State Chem.*, 2020, **288**, 121397.
46 L. Li, Q. Chen, Z. Niu, X. Zhou, T. Yang and W. Huang, *J. Mater. Chem. C*, 2016, **4**, 1900–1905.